JOURNAL OF COMPUTATIONAL PHYSICS **147,** 362–387 (1998)
ARTICLE NO. CP986093

A New Class of Time Discretization Schemes for the Solution of Nonlinear PDEs

Gregory Beylkin,*[,1] James M. Keiser,*[,2] and Lev Vozovoi†

**Department of Applied Mathematics, University of Colorado, Boulder, Colorado 80309-0526;*
†*School of Mathematical Sciences, Tel Aviv University, Tel Aviv 69978, Israel*
E-mail: beylkin@newton.colorado.edu

Received March 4, 1998; revised September 2, 1998

We consider issues of stability of time-discretization schemes with *exact* treatment of the *linear part* (ELP schemes) for solving nonlinear PDEs. A distinctive feature of ELP schemes is the exact evaluation of the contribution of the linear term, that is if the nonlinear term of the equation is zero, then the scheme reduces to the evaluation of the exponential function of the operator representing the linear term. Computing and applying the exponential or other functions of operators with variable coefficients in the usual manner requires evaluating dense matrices and is highly inefficient. It turns out that computing the exponential of strictly elliptic operators in the wavelet system of coordinates yields sparse matrices (for a finite but arbitrary accuracy). This observation makes our approach practical in a number of applications. In particular, we consider applications of ELP schemes to advection–diffusion equations. We study the stability of these schemes and show that both explicit and implicit ELP schemes have distinctly different stability properties if compared with known implicit–explicit schemes. For example, we describe explicit schemes with stability regions similar to those of typical implicit schemes used for solving advection–diffusion equations.

1. INTRODUCTION

In this paper we consider a new class of time-discretization schemes for solving nonlinear evolution equations,

$$u_t = \mathcal{L}u + \mathcal{N}(u), \tag{1.1}$$

where $\mathcal{L}$ represents the linear and $\mathcal{N}(\cdot)$ represents the nonlinear terms of the equation,

[1] The research was partially supported by ONR Grant N00014-91-J4037 and DARPA Grant F49620-93-1-0474.
[2] The research was partially supported by ONR Grant N00014-91-J4037.

0021-9991/98 $25.00

respectively. A distinctive feature of these new schemes is the exact evaluation of the contribution of the linear part. That is, if the nonlinear part is zero, then the scheme reduces to the evaluation of the exponential function of the operator (or matrix) $\mathcal{L}$ representing the linear part. We show that such schemes have very good stability properties and, in fact, describe explicit schemes with stability regions similar to those of typical implicit schemes used in, for example, fluid dynamics applications.

Computing and applying the exponential or other functions of operators in the usual manner typically requires evaluating dense matrices and, for that reason, is highly inefficient. An exception is the case where there is a (fast) transform that diagonalizes the operator. For example, if $\mathcal{L}$ is a convolution (or a circulant) matrix which is diagonalized by the Fourier transform (FT), then computing functions of operators can be accomplished by a fast algorithm, e.g. the FFT. It is clear that in this case the need for FT for the diagonalization prevents one from extending this approach to the case of variable coefficients.

We note that the problem of computing the exponential of large matrices has been of interest in numerical analysis (see, e.g. [11] and references therein) due to the ubiquitous nature of this operator in physics and mathematics. It turns out [5] that the wavelet transform produces sparse representations (up to a finite but arbitrary accuracy) for a wide class of operators. This fact may be used for computing functions of operators (see [5, 6]), in particular, of elliptic operators with variable coefficients. In the wavelet system of coordinates computing the exponential of such operators always results in sparse matrices and, therefore, using the exponential of operators for numerical purposes is an efficient option [7].

In this paper we further develop the approach of [7], concentrating on issues of stability of time-discretization schemes with *exact* treatment of the *linear part* (ELP) schemes. We study the stability of these schemes using an approach developed in [14] and show that ELP schemes have distinctly different stability properties as compared with known implicit–explicit schemes.

In particular, we are interested in applications of ELP schemes to advection–diffusion equations. Among equations for which ELP schemes appear to be very natural are, for example, the Navier–Stokes equations which may be written in the form (1.1) (see Appendix A). The stability properties of time-discretization schemes for advection–diffusion equations are controlled by the linear term and, therefore, these equations require an implicit treatment to avoid choosing an unreasonably small time step. As we show in this paper, using an explicit ELP scheme, it is possible to achieve stability usually associated with implicit predictor–corrector schemes. Even if an implicit ELP scheme is used, as is done in [7], an approximation is used only for the nonlinear term, giving one a chance to clearly distinguish numerical errors due to that term. Moreover, in the usual implicit schemes for advection–diffusion equations the corrector part of the scheme requires iterations that involve either both linear and nonlinear terms or only the linear term (see [14, 3]). It is well known that, due to the high condition number of the matrix representing the linear (diffusion) term, the fixed-point iteration is not a good option. More sophisticated and computationally more expensive choices are required, since otherwise the size of the time step is greatly reduced. Implicit ELP schemes do not involve the linear term and typically the fixed-point iteration is sufficient [7].

As we already pointed out, implementation of the new schemes requires applying functions of operators (e.g. the exponential). For a wide class of operators with nonconstant coefficients these functions are sparse in the wavelet system of coordinates (up to finite but arbitrary accuracy) and, for that reason, are best computed and applied in that domain.

A consistent adaptive approach may be used to perform all computations in the wavelet domain [7]. We note, however, that applying the exponential function of operators in the wavelet domain may also be combined with the evaluation of the nonlinear part in the physical domain. This may be the simplest way to implement ELP schemes, short of implementing adaptive schemes of [7]. ELP schemes may also be used in combination with pseudo-spectral methods in space. For example, using the pseudo-spectral Fourier method for solving equations with constant coefficients, differential operators can be applied in the Fourier domain and the nonlinear part in the physical domain.

In Section 2 we introduce new multistep methods where the linear part is treated exactly and the nonlinear part is evaluated either implicitly or explicitly. We introduce an integral representation for the time evolution problem and then discretize the integral equation in time. Finally, we derive expressions for the operator-valued coefficients representing contributions from different time levels. Then, in Section 3, we describe algorithms for the evaluation of the operator-valued coefficients and in Section 4 we study stability regions of new schemes. We describe a method for linear stability analysis following [14] and construct stability regions for the new class of schemes in order to analyze their properties.

2. SCHEMES WITH EXACT TREATMENT OF THE LINEAR TERM

2.1. *Integral Formulation*

We are interested in the solution of nonlinear evolution equations of the form

$$u_t = \mathcal{L}u + \mathcal{N}(u) \quad \text{in } \Omega \in \mathbb{R}^d, \tag{2.1}$$

where $u = u(x, t)$, $x \in \mathbb{R}^d$, $d = 1, 2, 3$, and $t \in [0, T]$. We also supply the initial conditions,

$$u(x, 0) = u_0(x) \quad \text{in } \Omega, \tag{2.2}$$

and the linear boundary conditions

$$\mathcal{B}u(x, t) = 0 \quad \text{on } \partial\Omega \in \mathbb{R}^{d-1}, t \in [0, T]. \tag{2.3}$$

An important example that we have in mind is advection–diffusion equations and, in particular, the Navier–Stokes equations which we rewrite in the form (2.1) in Appendix A. An adaptive scheme of ELP type has been used in [7] and in this paper we develop the formalism and study stability properties of such schemes in a more general setting.

We split the operator on the right-hand side of (2.1) into the linear part, $\mathcal{L}u$, and the nonlinear part, $\mathcal{N}(u)$. Following [7], we use the standard semigroup approach in order to convert the initial value problem (2.1), (2.2) to the nonlinear integral equation of the form

$$u(x, t) = e^{t\mathcal{L}}u(x, 0) + \int_0^t e^{(t-\tau)\mathcal{L}}\mathcal{N}(u(x, \tau))\, d\tau. \tag{2.4}$$

We note that the term $e^{t\mathcal{L}}u(x, 0)$ in (2.4) can always be replaced by $e^{(t-\eta)\mathcal{L}}u(x, \eta)$, $0 \le \eta \le t$, provided $u(x, \eta)$ is known. Such a form of the integral operator is slightly more general than that used in [7] (where $\eta = 0$). Choosing $\eta \neq 0$ allows us to study a wider class of ELP schemes and has a significant effect on their stability properties. A still more general

form of (2.4),

$$u(x,t) = \sum_{i=1}^{n} c_i e^{(t-\eta_i)\mathcal{L}} u(x,\eta_i) + \int_0^t e^{(t-\tau)\mathcal{L}} \mathcal{N}(u(x,\tau))\, d\tau, \quad \sum_{i=1}^{n} c_i = 1, \tag{2.5}$$

can be considered, where $u(x,\eta_i)$, $i, 1\ldots, n$, are assumed to be known (we use (2.5) with $n=1$).

The operator $\mathcal{L}$ and the exponential operator $e^{\mathcal{L}t}$ in (2.4) incorporate the boundary conditions. For example, writing $u(x,t) = e^{\mathcal{L}t}u_0(x)$ implies that the function $u(x,t)$ solves $u_t = \mathcal{L}u$ with the initial condition $u(x,0) = u_0(x)$ and the boundary condition $\mathcal{B}u(x,t) = 0$ for $x \in \partial\Omega$.

The integral equation (2.4) is easy to use for numerical purposes if, for example, $\mathcal{L}$ is an operator with constant coefficients and u is a periodic function. In this case $\mathcal{L}$ can be represented by a diagonal matrix in the Fourier basis. For instance, if $\mathcal{L}$ is the Laplacian and $u(x) = e^{ikx}$, then $\Delta u = -k^2 u$ and, in such a case, the exponential operator $e^{(t-\tau)\mathcal{L}}$ simply reduces to multiplication by $e^{-k^2(t-\tau)}$. However, for a general linear operator $\mathcal{L}$ with variable coefficients, the exponential operators appearing in this equation are represented by dense matrices. As far as we know, this is the main reason for the limited use of (2.4) as a starting point of numerical discretization.

We observe that the situation is different for the exponential operators on a wide class of linear operators in a wavelet system of coordinates. The sparsity of the exponential operators was utilized in [7] for constructing a numerical algorithm for the solution of PDEs of the form (2.1). In this paper we develop this approach further in order to construct a collection of high order discretizations of (2.4) with good stability properties.

2.2. *A Procedure for Time Discretization*

In order to simplify the notation in our derivation, we replace a linear operator $\mathcal{L}$ by a scalar q since the coefficients of the scheme are analytic (operator) functions of $\mathcal{L}$. Since all such functions commute with each other, it is sufficient to consider a scalar in deriving the coefficients of the numerical scheme.

Thus, instead of (2.1) and (2.4), it is sufficient to examine

$$u_t = qu + \mathcal{N}(u) \tag{2.6}$$

and

$$u(x,t) = e^{q(t-\eta)} u(x,\eta) + \int_0^t e^{q(t-\tau)} \mathcal{N}(u(x,\tau))\, d\tau, \tag{2.7}$$

where $0 \le \eta \le t$ and $u(x,\eta)$ is given.

Let us consider the function $u(x,t)$ at the discrete moments of time $t_n = t_0 + n\Delta t$, where Δt is the time step so that $u_n \equiv u(x,t_n)$ and $N_n \equiv \mathcal{N}(u(x,t_n))$. Discretizing (2.7) yields

$$u_{n+1} = e^{ql\Delta t} u_{n+1-l} + \Delta t \left(\gamma N_{n+1} + \sum_{m=0}^{M-1} \beta_m N_{n-m} \right), \tag{2.8}$$

where $M+1$ is the number of time levels involved in the discretization and $l \le M$. The expression in parenthesis in (2.8) may be viewed as the numerical quadrature for the integral

in (2.7). The coefficients γ and β_m are the functions of $q\Delta t$ (to simplify the notation, we suppress the dependence of γ and β_m on l).

We observe that the algorithm is explicit if $\gamma = 0$ and it is implicit otherwise. Typically, for a given M, the order of accuracy is M for an explicit scheme and $M+1$ for an implicit scheme, due to one more degree of freedom, γ (see later for a more detailed discussion). We refer to this family of schemes as exact linear part (ELP) schemes.

Remark 1. Using (2.8) to discretize partial differential equations (or, in general, using semigroup approach as in (2.4)) may be viewed as a way to "reduce" partial differential to ordinary differential equations. For example, one can apply the first Dahlquist criterion for (2.8) (see, e.g. [12]) to determine the maximal order for the implicit schemes. The reason this can be done is that the operator coefficients in (2.8) commute with each other and, thus, polynomials with such coefficients can be manipulated in the usual manner.

Remark 2. In the particular case where $l = 2$, $\gamma = 0$, and $M = 1$, Eq. (2.8) turns into the explicit scheme known as the "slave-frog" scheme,

$$u_{n+1} = e^{2q\Delta t}u_{n-1} + \Delta t\beta_0 N_n, \quad \beta_0 = \frac{e^{2q\Delta t} - 1}{q\Delta t}. \tag{2.9}$$

This scheme has been used in computational fluid dynamics (see, e.g. [9]). We do not know other examples of temporal schemes related to the family (2.8). As we will see below, the scheme in (2.9) does not have good stability properties (see Section 4.2).

Let us first consider the case $l = 1$ (so that $\eta = t_n$ in Eq. (2.7) is the nearest time level t_{n+1}),

$$u_{n+1} = e^{q\Delta t}u_n + \Delta t\left(\gamma N_{n+1} + \sum_{m=0}^{M-1}\beta_m N_{n-m}\right). \tag{2.10}$$

Our task now is to find the coefficients γ and β_m of scheme (2.10) in terms of $q\Delta t$. In [7] these coefficients are derived so that (i) the expression in parentheses is an $M+1$ order quadrature approximation to the integral in (2.7) and (ii) the quadrature uses the fewest number of nonzero coefficients, β_m. In this paper we adopt a different approach and obtain expressions for the coefficients γ and β_m in (2.10) by using the differential equation (2.6) and by expanding the terms u_{n+1} and $e^{q\Delta t}u_n$ into the Taylor series. The resulting expressions differ from those in [7] by higher order terms in $q\Delta t$ which are beyond the order of the approximation (see discussion below).

We start by expanding u_{n+1} in the Taylor series at the time level t_n,

$$u_{n+1} = \sum_{k=0}^{\infty} u_n^{(k)}\frac{(\Delta t)^k}{k!}, \tag{2.11}$$

where

$$u_n^{(k)} = \left.\frac{\partial^k}{\partial t^k}u(t)\right|_{t=t_n}.$$

The differential equation (2.6) yields relations between the derivatives of u and those of the nonlinear term, namely,

$$\begin{aligned} u^{(1)} &= qu + N, \\ u^{(2)} &= qu^{(1)} + N^{(1)} = q^2u + qN + N^{(1)}, \\ u^{(3)} &= q^3u + q^2N + qN^{(1)} + N^{(2)}, \end{aligned} \tag{2.12}$$

etc., and, in general,

$$u^{(k)} = q^k u + \sum_{j=0}^{k-1} N^{(j)} q^{k-1-j}. \tag{2.13}$$

Substituting (2.12) into (2.11), we have

$$\begin{aligned} u_{n+1} &= \sum_{k=0}^{\infty} q^k \frac{(\Delta t)^k}{k!} u_n + \sum_{k=1}^{\infty} \sum_{j=0}^{k} N^{(j)} q^{k-1-j} \frac{(\Delta t)^k}{k!} \\ &= e^{q\Delta t} u_n + \sum_{k=0}^{\infty} \sum_{j=0}^{k} N^{(j)} q^{k-j} \frac{(\Delta t)^{k+1}}{(k+1)!}. \end{aligned} \tag{2.14}$$

Changing the order of summation, we obtain

$$\begin{aligned} \sum_{k=0}^{\infty} \sum_{j=0}^{k} N^{(j)} q^{k-j} \frac{(\Delta t)^{k+1}}{(k+1)!} &= \sum_{j=0}^{\infty} N^{(j)} \sum_{k=j}^{\infty} q^{k-j} \frac{(\Delta t)^{k+1}}{(k+1)!} \\ &= \sum_{j=0}^{\infty} N^{(j)} (\Delta t)^{j+1} \left(\frac{1}{(q\Delta t)^{j+1}} \sum_{k=j+1}^{\infty} \frac{(q\Delta t)^k}{k!} \right) \\ &= \sum_{j=0}^{\infty} N^{(j)} (\Delta t)^{j+1} \mathrm{Q}_{j+1}(q\Delta t), \end{aligned} \tag{2.15}$$

where we denote

$$\mathrm{Q}_j(x) = \frac{\mathrm{e}^x - \mathrm{E}_j(x)}{x^j} \tag{2.16}$$

and where

$$\mathrm{E}_j(x) = \sum_{k=0}^{j-1} \frac{x^k}{k!} \tag{2.17}$$

is a truncated expansion of the exponential e^x. Thus, we obtain from (2.14) and (2.15),

$$u_{n+1} = \mathrm{e}^{q\Delta t} u_n + \Delta t \sum_{j=0}^{\infty} N^{(j)} (\Delta t)^j \mathrm{Q}_{j+1}(q\Delta t). \tag{2.18}$$

Also, for the nonlinear part of (2.10), we have

$$\gamma N_{n+1} + \sum_{m=0}^{M-1} \beta_m N_{n-m} = \sum_{j=0}^{\infty} N^{(j)} \frac{(\Delta t)^j}{j!} \left(\gamma + (-1)^j \sum_{m=0}^{M-1} \beta_m m^j \right), \tag{2.19}$$

where we expand N_{n+1} and N_{n-m} around the time level t_n. Substituting (2.18) and (2.19) into (2.10), we obtain equations for the coefficients γ and β_m. In the implicit case $\gamma \neq 0$

TABLE I
Coefficients of Implicit ELP Schemes for $l = 1$, where $Q_k = Q_k(q\Delta t)$

M	γ	β_0	β_1	β_2	Order
1	Q_2	$Q_1 - Q_2$	0	0	2
2	$Q_2/2 + Q_3$	$Q_1 - 2Q_3$	$Q_3 - Q_2/2$	0	3
3	$Q_2/3 + Q_3 + Q_4$	$Q_1 + Q_2/2 - 2Q_3 - 3Q_4$	$-Q_2 + Q_3 + 3Q_4$	$Q_2/6 - Q_4$	4

and we have

$$\begin{aligned} \gamma + \sum_{m=0}^{M-1} \beta_m &= Q_1 \\ \frac{1}{k!}\left(\gamma + (-1)^k \sum_{m=1}^{M-1} m^k \beta_m\right) &= Q_{k+1}, \quad k = 1, \ldots, M. \end{aligned} \tag{2.20}$$

In the explicit case $\gamma = 0$ and we obtain

$$\begin{aligned} \sum_{m=0}^{M-1} \beta_m &= Q_1, \\ \frac{(-1)^k}{k!} \sum_{m=1}^{M-1} m^k \beta_m &= Q_{k+1}, \quad k = 1, \ldots, M-1. \end{aligned} \tag{2.21}$$

For $l = 1$ we provide Tables I and II for $M = 1, 2, 3$ with expressions for the coefficients of the implicit ($\gamma \neq 0$) and the explicit ($\gamma = 0$) schemes in terms of $Q_k = Q_k(q\Delta t)$.

For any l, $1 < l \leq M$, in (2.8), we can repeat the above considerations and obtain coefficients of the corresponding scheme. In Tables III and IV we provide the coefficients of implicit and explicit schemes in the case $l = 2$ in terms of $Q_k^2 = Q_k(2q\Delta t)$ for $M = 1, 2, 3$.

The prescribed number of time levels M in the discretization scheme (2.8) determines the order of the scheme. Usually, implicit schemes ($\gamma \neq 0$) are of order $(q\Delta t)^{M+1}$, whereas explicit schemes ($\gamma = 0$) are of order $(q\Delta t)^M$. However, there might be exceptions due to a symmetry. For example, the explicit scheme (2.9) with $\gamma = 0$, $l = 2$, and $M = 1$ is of second order, since the first-order terms cancel when we expand u_{n+1} and u_{n-1} at the time level t_n.

Remark 3. Although for a given M, systems (2.20) and (2.21) have unique solutions, the terms on the right-hand side, Q_k, can be modified by adding terms of higher orders (the order depends on k). These additional terms appear as contributions of higher order terms in the discretized integral equation (2.8). For example, in (2.20) we can perturb Q_{M+1} by a term of $O(q\Delta t)$, Q_M by a term of $O((q\Delta t)^2), \ldots,$ Q_1 by a term of $O((q\Delta t)^{M+1})$, without

TABLE II
Coefficients of Explicit ELP Schemes for $l = 1$, where $Q_k = Q_k(q\Delta t)$

M	β_0	β_1	β_2	Order
1	Q_1	0	0	1
2	$Q_1 + Q_2$	$-Q_2$	0	2
3	$Q_1 + 3Q_2/2 + Q_3$	$-2(Q_2 + Q_3)$	$Q_2/2 + Q_3$	3

TABLE III
Coefficients of Implicit ELP Schemes for $l = 2$, where $Q_k^2 = Q_k(2q\Delta t)$

M	γ	β_0	β_1	β_2	Order
1	$Q_2^2 - Q_1^2$	$2Q_1^2 - Q_2^2$	0	0	2
2	$Q_3^2 - Q_2^2/2$	$2(Q_2^2 - Q_3^2)$	$Q_1^2 - 3Q_2^2/2 + Q_3^2$	0	3
3	$-Q_2^2/6 + Q_4^2$	$Q_2^2 + Q_3^2 - 3Q_4^2$	$Q_1^2 - Q_2^2/2 - 2Q_3^2 + 3Q_4^2$	$-Q_2^2/3 + Q_3^2 - Q_4^2$	4

changing the order of the resulting scheme. Adopting terminology used in perturbation theory, we refer to the coefficients of the schemes obtained as solutions of (2.20) and (2.21) as "bare," and the coefficients obtained as solutions of the perturbed equations as "modified." Such modified coefficients were used in [7]. Although the order of the scheme does not change if one uses modified coefficients instead of bare coefficients, it turns out that the stability properties are rather sensitive to such perturbations. Let us also mention here that some schemes in [7] use modified coefficients (in our sense) in combination with mixing time levels within the nonlinear part. We note that such schemes cannot be obtained with the formalism presented here since they depend on the particular form of the nonlinear term.

Remark 4. The nonlinear term in Eq. (2.6) may consist of several parts that can be treated differently. Suppose that the nonlinear term is split into two parts,

$$u_t = qu + \mathcal{N}^{(I)}(u) + \mathcal{N}^{(II)}(u),$$

and, therefore, the discretized equation (e.g., in the case $l = 1$) has the form

$$u_{n+1} = e^{q\Delta t}u_n + \Delta t\left(\gamma^{(I)}N_{n+1}^{(I)} + \sum_{m=0}^{M_I-1}\beta_m^{(I)}N_{n-m}^{(I)}\right) + \Delta t\left(\gamma^{(II)}N_{n+1}^{(II)} + \sum_{m=0}^{M_{II}-1}\beta_m^{(II)}N_{n-m}^{(II)}\right).$$

Using previous considerations, we can show that each group of coefficients $\{\gamma^{(I)}, \beta^{(I)}\}$ and $\{\gamma^{(II)}, \beta^{(II)}\}$ independently satisfy (2.20). For example, we can use an explicit scheme for the first part with $\gamma^{(I)} = 0$ and an implicit scheme for the second one with $\gamma^{(II)} \neq 0$.

3. EVALUATION OF THE OPERATOR-VALUED QUADRATURE COEFFICIENTS

The key point in our approach is an observation that operator-valued quadrature coefficients can be represented by sparse matrices (for a finite but arbitrary accuracy). Thus, in order to make ELP schemes practical we have to provide an algorithm for their evaluation.

TABLE IV
Coefficients of Explicit ELP Schemes for $l = 2$, where $Q_k^2 = Q_k(2q\Delta t)$

M	β_0	β_1	β_2	Order
1	Q_1^2	0	0	2
2	Q_2^2	$Q_1^2 - Q_2^2$	0	2
3	$Q_2^2/2 + Q_3^2$	$Q_1^2 - 2Q_3^2$	$-Q_2^2/2 + Q_3^2$	3

As we have shown in Section 2, the coefficients of ELP schemes are written in terms of operators $Q_k = Q_k(\mathcal{L}\Delta t)$, where

$$Q_j(\mathcal{L}\Delta t) = \frac{e^{\mathcal{L}\Delta t} - E_j(\mathcal{L}\Delta t)}{(\mathcal{L}\Delta t)^j}, \tag{3.1}$$

and

$$E_j(\mathcal{L}\Delta t) = \sum_{k=0}^{j-1} \frac{(\mathcal{L}\Delta t)^k}{k!}, \tag{3.2}$$

for $j = 0, 1, \ldots$. We have

$$\begin{aligned} Q_0(\mathcal{L}\Delta t) &= e^{\mathcal{L}\Delta t}, \\ Q_1(\mathcal{L}\Delta t) &= (e^{\mathcal{L}\Delta t} - \mathcal{I})(\mathcal{L}\Delta t)^{-1}, \\ Q_2(\mathcal{L}\Delta t) &= (e^{\mathcal{L}\Delta t} - \mathcal{I} - \mathcal{L}\Delta t)(\mathcal{L}\Delta t)^{-2}, \\ &\cdots \end{aligned} \tag{3.3}$$

We will now describe a method that permits us to compute operators $Q_0, Q_1, Q_2, \ldots$ without computing $(\mathcal{L}\Delta t)^{-1}$. The problem in using the Taylor expansion directly is that it will result in a loss of accuracy due to possibly large singular values of $\mathcal{L}\Delta t$. To avoid this problem in computing the exponential Q_0, we use the scaling and squaring method. This method results in a fast algorithm if the evaluation is performed in a wavelet basis with a sufficient number of vanishing moments (for a chosen accuracy) [6].

The scaling and squaring method for the exponential is based on the identity

$$Q_0(2x) = Q_0^2(x). \tag{3.4}$$

First we compute $Q_0(\mathcal{L}\Delta t 2^{-l})$ for some l chosen so that the largest singular value of $\mathcal{L}\Delta t 2^{-l}$ is less than one. This computation is performed using the Taylor expansion. Using (3.4), the resulting matrix is then squared l times to obtain the final answer.

A similar algorithm may be used for computing $Q_j(\mathcal{L}\Delta t)$, $j = 1, 2, \ldots$, for any finite j. Let us illustrate this approach by considering $j = 1, 2, \ldots, 6$.

It is not difficult to verify that

$$\begin{aligned} Q_1(2x) &= \frac{1}{2}(Q_0(x)Q_1(x) + Q_1(x)), \\ Q_2(2x) &= \frac{1}{4}(Q_1(x)Q_1(x) + 2Q_2(x)), \\ Q_3(2x) &= \frac{1}{8}(Q_1(x)Q_2(x) + 2Q_3(x) + Q_2(x)), \\ Q_4(2x) &= \frac{1}{16}(Q_2(x)Q_2(x) + 2Q_4(x) + 2Q_3(x)), \\ Q_5(2x) &= \frac{1}{32}\left(Q_2(x)Q_3(x) + 2Q_5(x) + 2Q_4(x) + \frac{1}{2}Q_3(x)\right), \\ Q_6(2x) &= \frac{1}{64}(Q_3(x)Q_3(x) + 2Q_6(x) + 2Q_5(x) + Q_4(x)), \\ &\cdots \end{aligned} \tag{3.5}$$

The identities in (3.5) are obtained by considering the difference between $2^j Q_j(2x)$ and $Q_{j/2}(x)Q_{j/2}(x)$ if j is even, and $Q_{(j-1)/2}(x)Q_{(j+1)/2}(x)$ if j is odd. This difference is then expressed using a linear combination of $Q_j(x), Q_{j-1}(x), \ldots$.

Thus, a modified scaling and squaring method for computing operator-valued quadrature coefficients for ELP schemes starts by the computation of $Q_0(\mathcal{L}\Delta t 2^{-l})$, $Q_1(\mathcal{L}\Delta t 2^{-l})$, $Q_2(\mathcal{L}\Delta t 2^{-l}), \ldots$ for some l selected so that the largest singular value of all three operators is less than one. For this evaluation we use the Taylor series. We then proceed by using the identities in (3.4) and (3.5) l times to compute the operators for the required value of the argument.

The speed of the evaluation and application of operator-valued coefficients in spatial dimensions two and three is one of the important factors in the practicality of ELP schemes. Although the algorithms described above scale properly with size in all dimensions, establishing ways of reducing constants in operation counts remains an important task in dimensions two and three. We will address these issues in a separate paper.

4. STABILITY ANALYSIS

4.1. *Preliminary Considerations*

The standard linear stability analysis of discrete schemes (see, e.g. [8]) deals with a test problem,

$$u_t = \mu u, \tag{4.1}$$

where $\mu = \mu_r + i\mu_i$ is a complex number. Applying a discretization method to Eq. (4.1), we obtain a homogeneous linear difference equation,

$$\sum_{k=0}^{M} (\alpha_k u_{n-k} - \mu \Delta t \beta_k u_{n-k}) = 0 \tag{4.2}$$

which is solved explicitly. We then consider a region in the complex μ-plane where the solution of the discretized equation (4.2) is bounded as $n \to \infty$ (n is the number of time steps). This region of (absolute) stability may be compared to the actual region of decay and growth of solutions of (4.1) in order to ascertain the properties of the numerical scheme.

In the stability analysis of the ELP method we adopt an extension of the approach suggested in [14]. The proposal of [14] is to compute a family of curves (boundaries of stability regions) for a more general test problem,

$$u_t = -qu + \mu u, \tag{4.3}$$

where different curves correspond to different values of q. The point is that the first and second terms on the right-hand side of (4.3) may be discretized using different schemes. For example, these two terms may represent linear and nonlinear parts of the differential equation. For a fixed q the analysis proceeds as in the standard method.

If we discretize the test problem (4.3), then parameters q and μ will appear in combination with the time step Δt. Let us fix the parameter $q\Delta t$ and plot the family of boundaries of stability regions in the complex plane $(\mu_r \Delta t, \mu_i \Delta t)$, where $\mu = \mu_r + i\mu_i$. A technique of computing the boundaries of stability regions is described in Appendix B.

We start by providing several examples of stability diagrams for discretization methods discussed in [14] in order to establish a baseline for comparison with the stability properties of ELP schemes.

Let us first provide an interpretation for parameters q and μ for a model advection–diffusion equation,

$$u_t = \alpha u_{xx} + U u_x, \tag{4.4}$$

where U is a constant convective velocity and $\alpha > 0$ is a damping constant. Considering periodic boundary conditions, we obtain for the Fourier transform $\hat{u}$ of the function u,

$$\hat{u}_t = -\alpha k^2 \hat{u} + ikU\hat{u}. \tag{4.5}$$

The equation (4.5) has the same structure as Eq. (4.3) with $q = \alpha k^2 > 0$ and $\mu = ikU$. For nonlinear equations under consideration the splitting of the right-hand side of (4.5) into two terms corresponds to the splitting into linear (diffusion) and nonlinear (advection) parts, respectively.

We now turn to an example from [14] which deals with a mixed implicit–explicit method, where the linear term is approximated using the implicit third-order Adams–Moulton scheme and the nonlinear term is approximated using the explicit third-order Adams–Bashforth scheme as

$$u_n = u_{n-1} - q\Delta t \sum_{k=0}^{2} \alpha_k u_{n-k} + \mu \Delta t \sum_{k=1}^{3} \beta_k u_{n-k}, \tag{4.6}$$

where $\alpha_0 = 5/12$, $\alpha_1 = 8/12$, $\alpha_2 = -1/12$, and $\beta_1 = 23/12$, $\beta_2 = -16/12$, $\beta_3 = 5/12$. The corresponding stability diagram is plotted in Fig. 1. We observe that this method is conditionally stable with a region of stability that separates from the imaginary (vertical) axis for $q\Delta t \geq 6$ (that is, for high wavenumbers, since $q \propto k^2$). In this figure, as well as other stability diagrams below, the label of the curve (the boundary of the stability region), $q\Delta t$, can be identified by finding the point of intersection of the corresponding curve with the horizontal axis in the right half-plane.

In our second example, borrowed from the same paper [14], we reproduce the stability diagram for a third-order stiffly stable scheme. According to [10], a method is stiffly stable if it is consistent in a neighborhood of the origin and absolutely stable away from the origin in the left imaginary plane. Stiffly stable multistep methods are implicit and their coefficients are available up to eleventh order (see [13]).

In [14] a mixed explicit–implicit stiffly stable scheme has been introduced,

$$\sum_{k=0}^{3} \alpha_k u_{n-k} = -q\Delta t u_n + \mu \Delta t \sum_{k=1}^{3} \beta_k u_{n-k}, \tag{4.7}$$

with α-coefficients being those of the standard third-order stiffly stable scheme from [10], $\alpha_0 = 11/6$, $\alpha_1 = -3$, $\alpha_2 = 3/2$, and $\alpha_3 = 1/3$. The coefficients for the explicit part are $\beta_1 = 3$, $\beta_2 = -3$, and $\beta_3 = 1$. The corresponding stability diagram is shown in Fig. 2. The stability region of this scheme is significantly broader than that of the third-order Adams–Moulton/Adams–Bashforth family in Fig. 1. We note that a larger amount of dissipation, q, stabilizes the convection term, i.e., the region of stability increases along the vertical (imaginary) axis as q becomes larger.

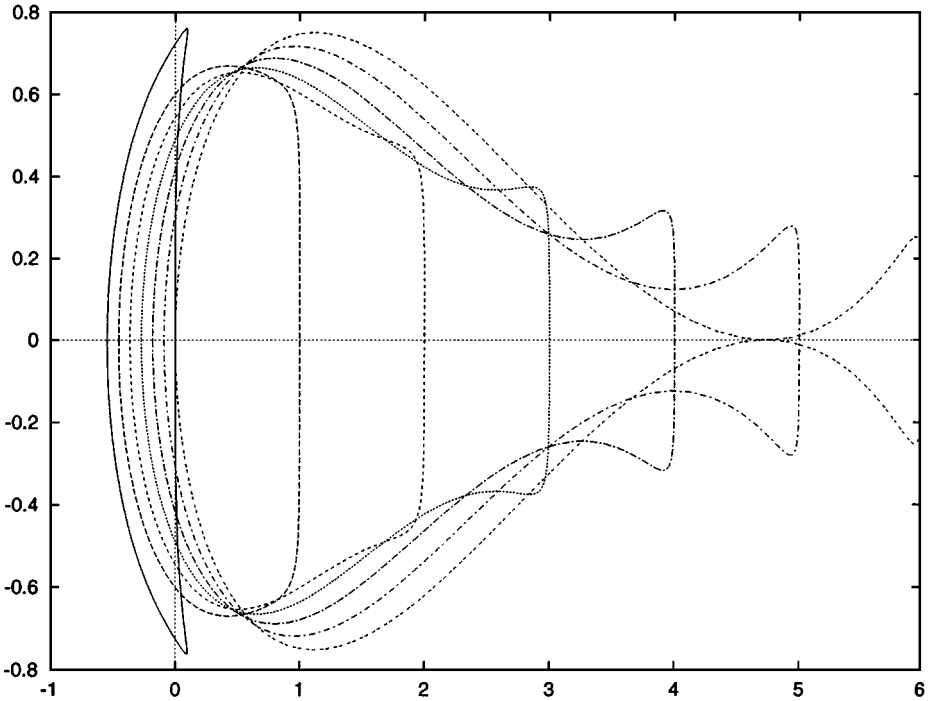

FIG. 1. Stability diagram of the third-order Adams–Moulton/Adams–Bashforth scheme. The curves correspond to different values of the parameter $q\Delta t$ ($q\Delta t = 0$ corresponds to the explicit scheme). This plot reproduces Fig. 6 in [14].

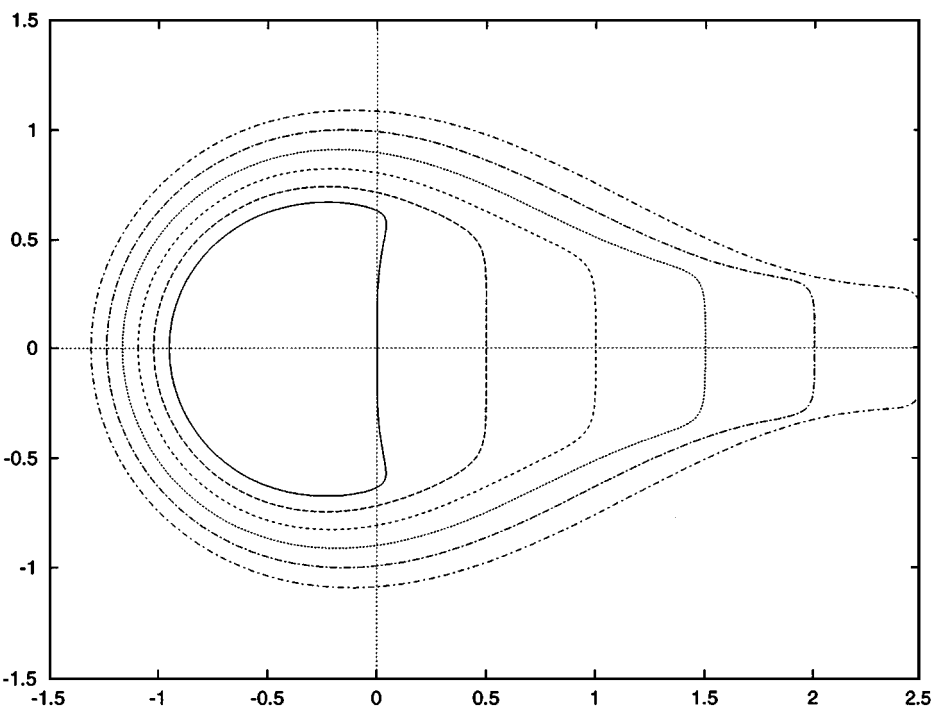

FIG. 2. Stability diagram of the mixed implicit–explicit stiffly stable scheme of third order ($q\Delta t = 0$ corresponds to the explicit scheme). This plot reproduces Fig. 7 in [14].

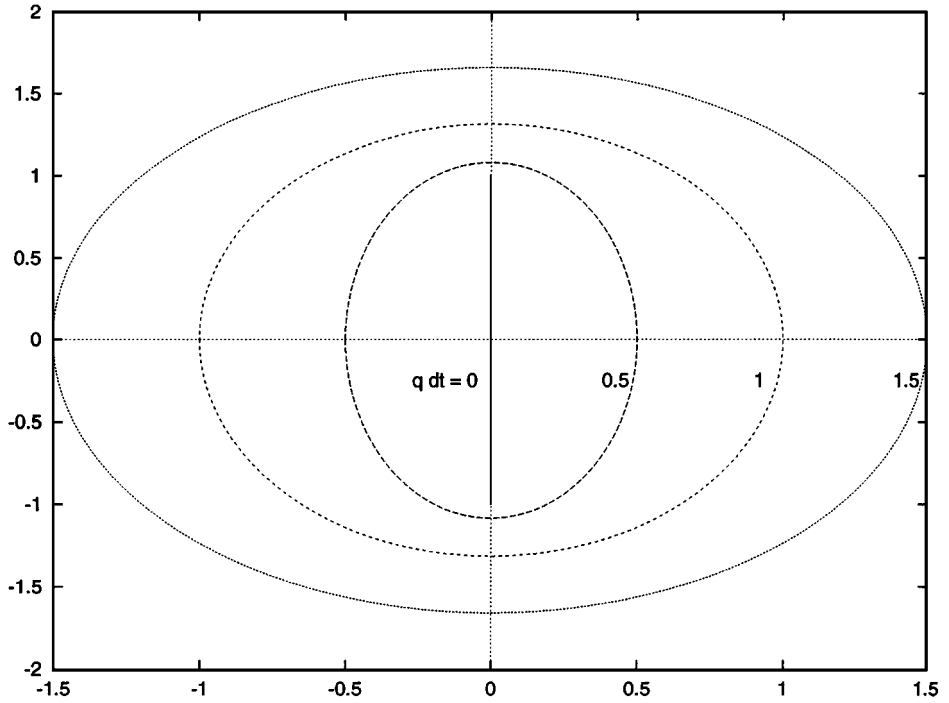

FIG. 3. Stability diagram for the scheme (2.9) with $l = 2$, $M = 1$ (slave-frog). The region of (absolute) stability collapses to the vertical line as $q\Delta t \to 0$.

4.2. *Stability Analysis of ELP Schemes*

We start our analysis with the "slave-frog" type schemes, which we obtain by setting $l = 2$ in (2.8). It turns out that the weak instability with respect to long waves known for the classical slave-frog scheme (2.9) with $M = 1$, also appears to be typical for other schemes of this family (at least for the most practical, with $M = 2$ and 3). We then consider a class of ELP schemes where $l = 1$ with significantly better stability properties.

Family of ELP schemes with $l = 2$. We display the regions of (absolute) stability for the second-order explicit scheme (2.9) in Fig. 3. As the parameter $q \to 0$, the stability region shrinks to the line on the imaginary axis. This is expected since in the limit $q \to 0$, Eq. (2.9) turns into the explicit midpoint scheme, which is known to be stable only on an interval of the imaginary axis (see, e.g. [8]). Therefore, this scheme does not provide enough dissipation for small q (or for the long waves if we have in mind the model problem (4.4)). Nevertheless, (2.9) has been used for numerical solution of some CFD problems. In order to overcome a weak instability with respect to the long waves, some additional ad-hoc "tricks" have been invented, such as "mixing" (from time to time) the contribution from several previous time levels. However, the problem with such ad-hoc approaches is that they severely decrease the accuracy of the method.

From our analysis it is clear that the weak instability at $q \ll 1$ is a common problem for all schemes where $l = 2$. In Fig. 4 we show the stability region for the third-order implicit scheme ($l = 2$, $M = 2$; see Table 3). Again, as $q \to 0$ the region of stability collapses to the vertical line.

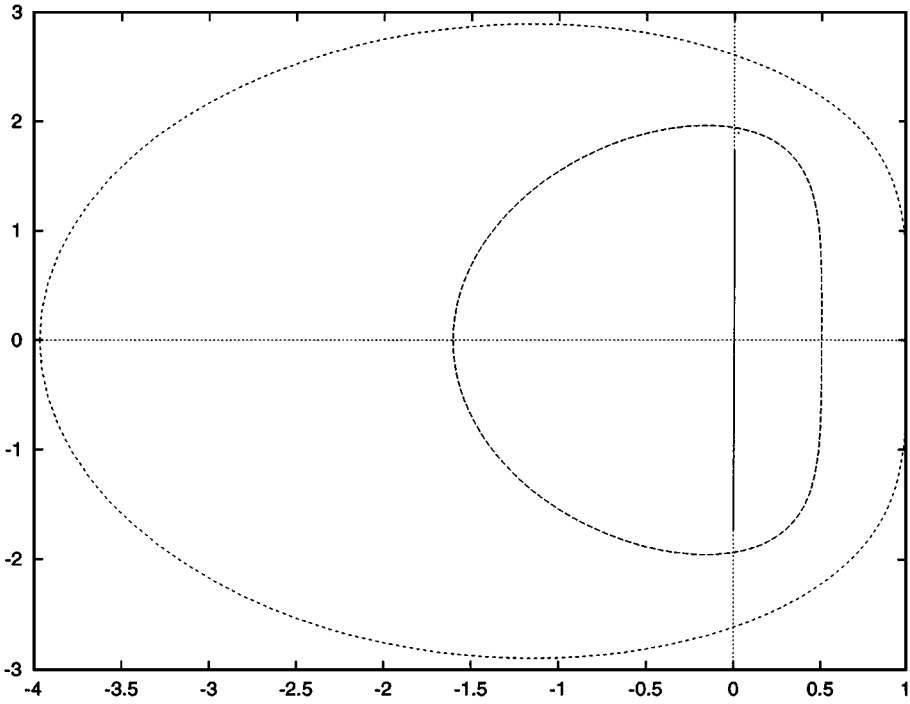

FIG. 4. Stability diagram for the implicit third-order scheme with $l = 2$, $M = 2$ (see Table III).

We provide in Appendix C an explanation for such behavior of the stability region of the $l = 2$ schemes in the limit $q \to 0$. We now turn to a class of schemes with better stability properties.

Implicit ELP schemes ($l = 1$). We start by showing in Fig. 5 the stability diagram for the second-order scheme ($l = 1$, $M = 1$; see Table I). The region of absolute stability includes the entire left half-plane and also a part of the right half-plane. In the limit $q \to 0$ the stability region coincides with the left half-plane.

This stability diagram is obtained using the bare coefficients (see Remark 3 in Section 2.2), namely, $\gamma = Q_2$ and $\beta_0 = Q_1 - Q_2$ in (2.10). If, instead, we use modified coefficients, choosing them as $\tilde{\gamma} = 1/2$ and $\tilde{\beta}_0 = Q_1/2$, then the stability boundaries become the vertical straight lines, intersecting the horizontal axis at the distance $q\Delta t$ to the right of the origin as shown in Fig. 6. The coefficients $\tilde{\gamma} = 1/2$ and $\tilde{\beta}_0 = Q_1/2$ satisfy the first equation in (2.20) and the second equation in (2.20) with $k = 1$, where Q_2 is perturbed by an $O(q\Delta t)$ term. This scheme was used in [7] and its stability diagram corresponds to an A-stable scheme (see e.g. [8]). Such schemes have the same stability regions as the differential equation (4.3) of the test problem, namely, the solution decays for $\mu_r - q < 0$ and it grows otherwise. The A-stability of this scheme is shown analytically in Appendix D.

The stability diagram for the third-order implicit scheme with the exact coefficients from Table I is plotted in Fig. 7. The stability region is much larger than that of the third-order stiffly stable scheme in Fig. 2. Moreover, at $q\Delta t = 2$ the stability boundary turns into a straight (vertical) line, and for $q\Delta t > 2$ all the left half-plane and a part of the right half-plane become stable (the scheme is super-stable with respect to high wave numbers). The "islands" of instability in the right half-plane contract as $q\Delta t$ increases. The stability region

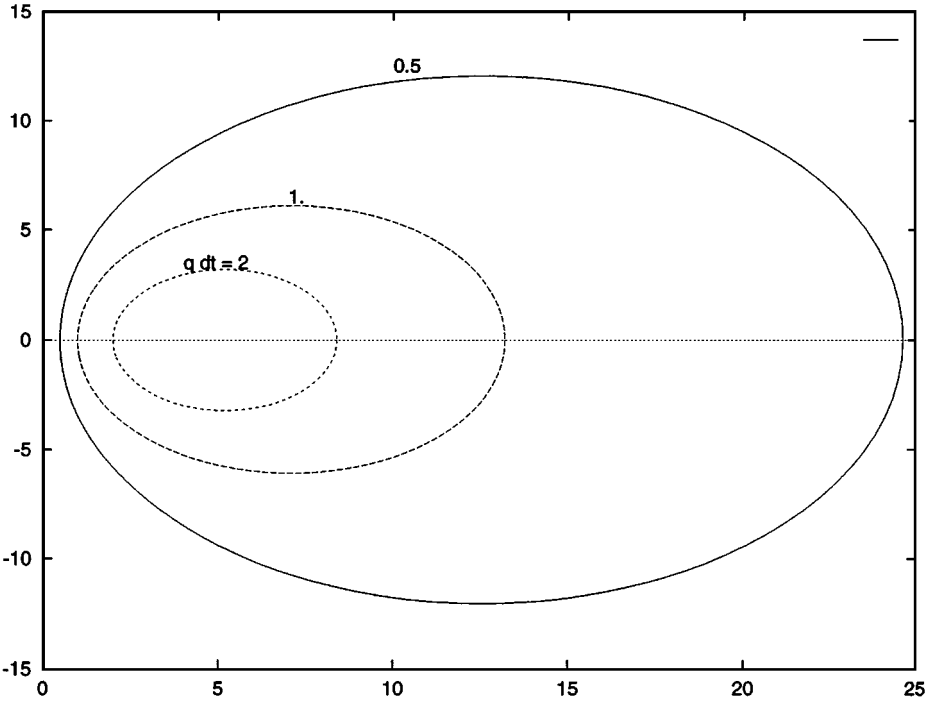

FIG. 5. Stability diagram for the second-order implicit scheme ($M = 1, l = 1$) using bare coefficients $\gamma = Q_2$ and $\beta_0 = Q_1 - Q_2$ from Table I. (Here the interior of the curves are the regions of *instability*.)

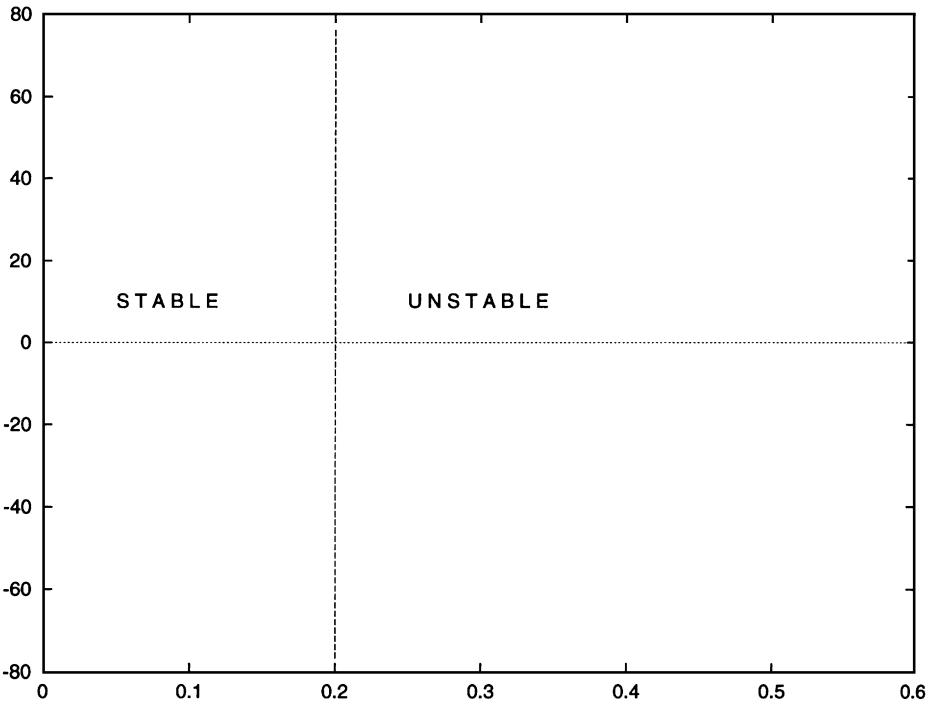

FIG. 6. Stability diagram for the second-order ELP implicit scheme ($M = 1, l = 1$) with modified coefficients $\tilde{\gamma} = \tilde{\beta}_0 = Q_1/2$ (A-stable scheme).

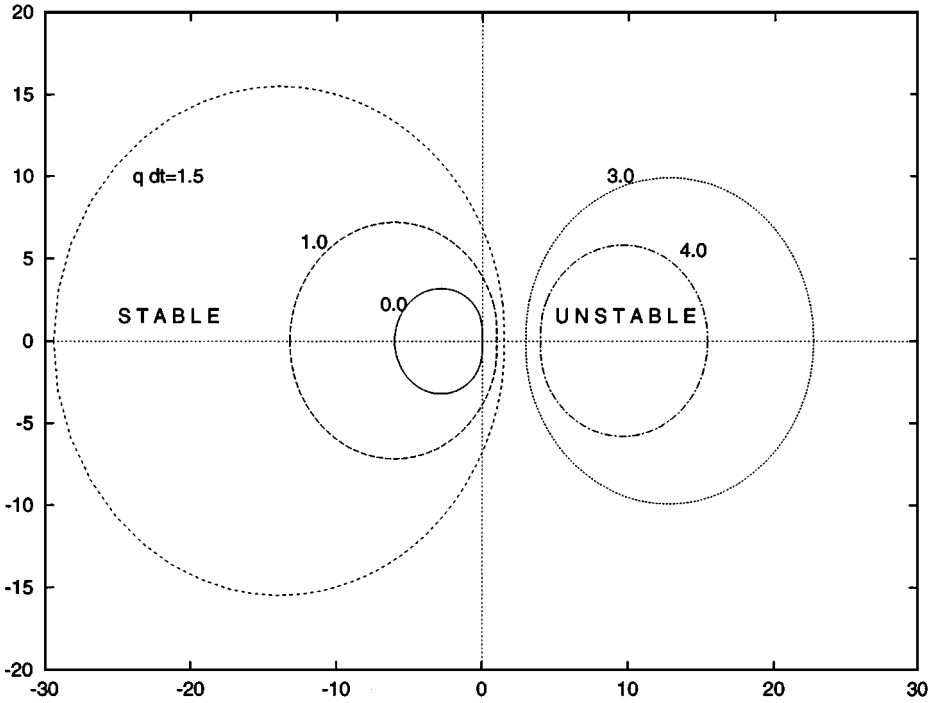

FIG. 7. Stability diagram for the third-order implicit scheme with $l = 1$, $M = 2$ and coefficients from Table I.

of the fourth-order implicit scheme is shown in Fig. 8. It is still larger than that of the third-order stiffly stable scheme. This scheme becomes super-stable for $q\Delta t > 4.26$ (not shown in Fig. 8).

Explicit ELP schemes ($l = 1$). Finally, we consider the stability of explicit ELP schemes. Let us illustrate the stability regions of the second $M = 2$ and third $M = 3$ order schemes in Figs. 9 and 10. We note that the stability regions of these schemes for $q\Delta t > 0$ are more reminiscent of those for implicit schemes (compare, for example, Fig. 10 with Fig. 2). In the limit $q\Delta t \to 0$ the stability regions tend to those of the second- and third-order Adams–Bashforth schemes. This is expected since in (2.8) the exponential function $e^{q\Delta t} \to 1$ as $q\Delta t \to 0$, and the bare coefficients β_k in (2.10) coincide with those of the corresponding order Adams–Bashforth scheme.

For useful schemes it is important that the stability regions obtained via the stability analysis of [14] grow as $q\Delta t$ becomes larger as, for example, in Fig. 2. In explicit ELP schemes the region of stability grows for large $q\Delta t$ (although for the third-order scheme this growth is not monotonic; as $q\Delta t$ varies from 0 to 1, the stability region shrinks somewhat and then starts to increase).

Let us compare the stability diagrams of the third-order explicit scheme with $M = 3$, $l = 1$, and coefficients from Table II in Fig. 10 with that of the mixed implicit–explicit stiffly stable scheme of third order from [14] in Fig. 2. This comparison shows that the explicit scheme will require a time step only about one-half of that of the implicit scheme in order to stay within the stability region. This is where ELP schemes may have an advantage since they do not require potentially expensive solves at each time step (especially in dimensions two and three).

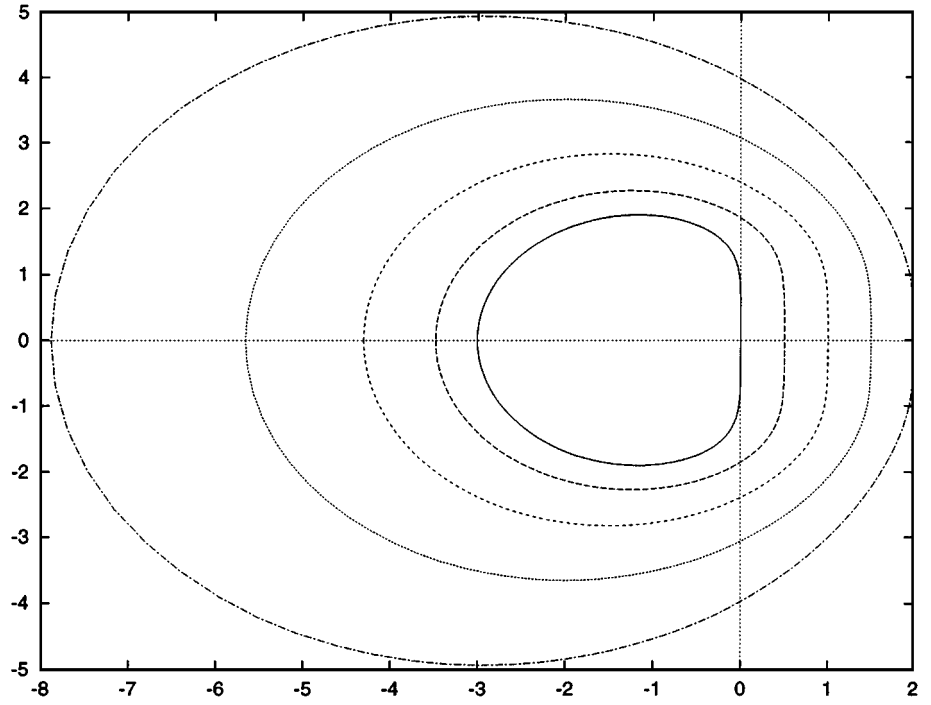

FIG. 8. Stability diagram for the fourth-order implicit scheme with $l = 1$, $M = 3$ and coefficients from Table I.

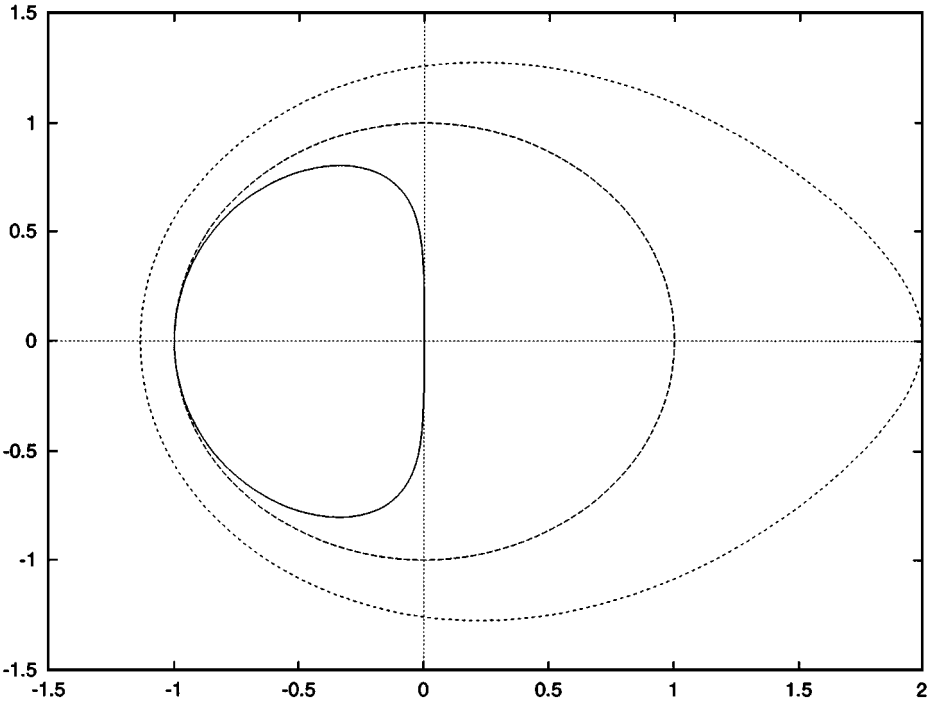

FIG. 9. Stability diagram for the second-order explicit scheme with $M = 2$, $l = 1$ and coefficients from Table II. The curve at $q\Delta t = 0$ corresponds to the boundary of the stability region of the second-order Adams–Bashforth method.

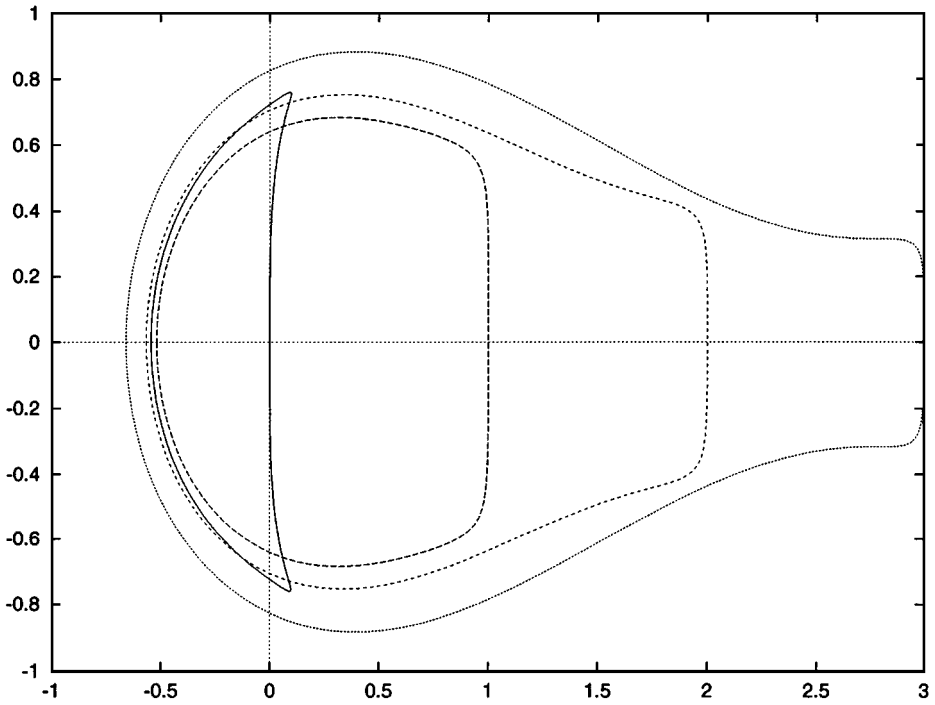

FIG. 10. Stability diagram for the third-order explicit scheme with $M = 3$, $l = 1$ and coefficients from Table II. The curve at $q\Delta t = 0$ corresponds to the boundary of the stability region of the third-order Adams–Bashforth method.

In the ordinary explicit methods, due to stability restrictions, the time step Δt is proportional to $(1/N)^2$, where N is the number of degrees of freedom in the spatial discretization (e.g. the number of grid points or the number of terms in spectral expansions, $N \propto k$). In the explicit ELP schemes the time step may be chosen to be proportional to $1/N$, as indicated by the stability diagrams and the above comparison with an implicit scheme.

EXAMPLE 1. Let us first consider a nonlinear diffusion equation with a forcing term,

$$u_t = \alpha u_{xx} - uu_x + f(x,t), \quad x \in [0,1]. \tag{4.8}$$

For tests we select

$$u^{(ref)} = \cos(t)\sin(2\pi\omega x), \tag{4.9}$$

as a solution and generate the corresponding forcing term $f(x,t)$. We then solve (4.8) with this forcing term. For the space discretization we write the solution in multiwavelet bases [1] using representations of differential operators and of the exponential of differential operators constructed in [2].

We use explicit ELP schemes of the first, second, and third orders and plot in Fig. 11 the numerical error as a function of time for $\alpha = 1$, $\omega = 3$. The time step is $\Delta t = 10^{-3}$. By choosing the number of subintervals $n = 16$ and the order of multiwavelets $k = 6$, we make the temporal errors dominant in this example.

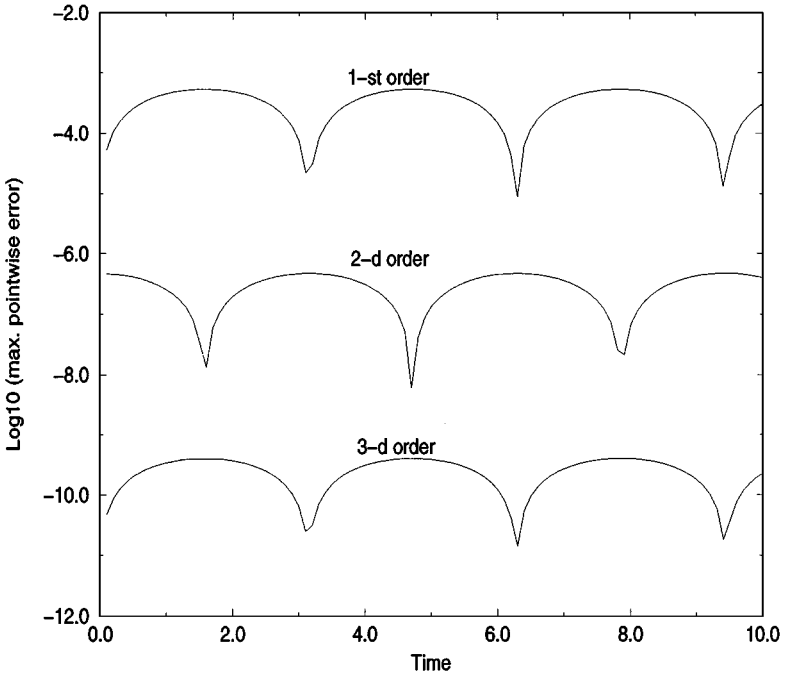

FIG. 11. Error as a function of time for Example 1 for first-, second-, and third-order explicit ELP schemes.

EXAMPLE 2. Again using explicit ELP schemes in time and multiwavelets in space, we consider Burgers' equation

$$u_t = \nu u_{xx} - u u_x, \quad x \in [0, 1]. \tag{4.10}$$

A reference solution with periodic boundary conditions may be written as

$$u^{(ref)} = -2\nu \frac{\phi_x(x - ct, t + \tau)}{\phi(x - ct, t + \tau)}, \quad \tau > 0 \tag{4.11}$$

where

$$\phi(x, t) = \sum_{n=-\infty}^{\infty} e^{-(x-n)^2/4\nu t}. \tag{4.12}$$

In Fig. 12 we display the numerical solution for $c = 4$, $\nu = 0.1/\pi$, and $\tau = 1/(2\pi)$ (these are parameters of the standard test case) so that the profile moves at speed $c = 4$. The pointwise numerical error for the solution at $t = 1/16$ is plotted in Fig. 13. The maximum numerical error is given in Table V for the explicit first-, second-, and third-order ELP

TABLE V
Maximum Error of the Solution of the Periodic Burgers' Equation at the Time $t = 1/16$, $\nu = 0.1/\pi$, and $c = 0, 4$

c\order	First	Second	Third
0	9.6×10^{-4}	3.6×10^{-7}	5.9×10^{-10}
4	3.0×10^{-2}	4.2×10^{-4}	6.5×10^{-6}

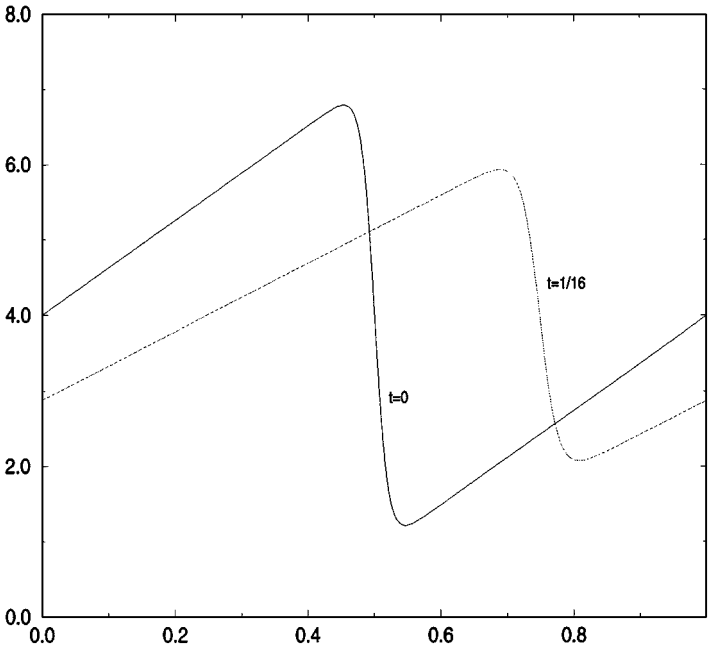

FIG. 12. Solution of the periodic Burgers' equation at $t = 0$ and $t = 1/16$; $\nu = 0.1/\pi$, $c = 4$.

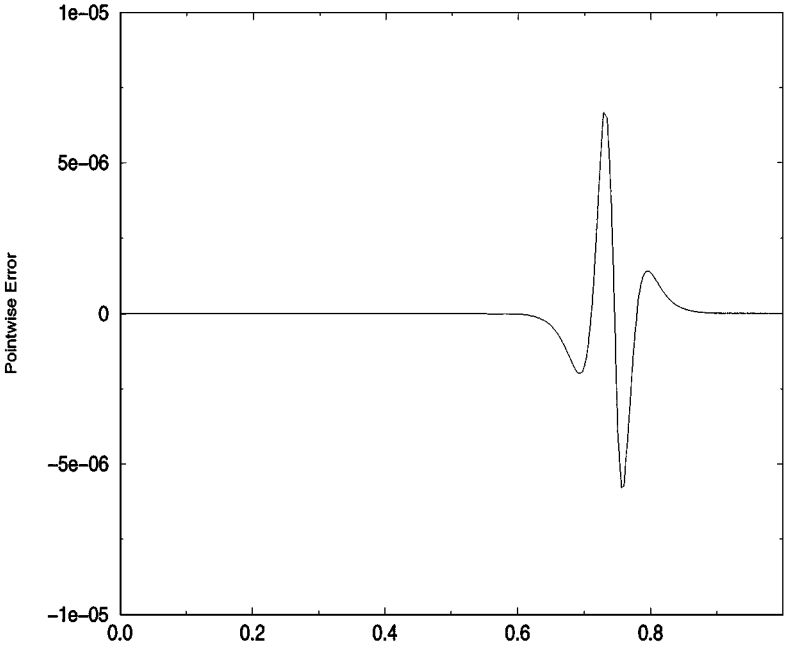

FIG. 13. The pointwise error for the solution of periodic Burgers' equation at $t = 1/16$.

schemes for $\Delta t = 10^{-4}$, $t = 1/16$ and $c = 0$, $c = 4$. Again, the spatial resolution was chosen to make temporal errors dominant.

5. CONCLUSIONS

We have demonstrated excellent stability properties of both explicit and implicit ELP schemes. The efficiency of using ELP schemes for nonlinear partial differential equations depends on the sparsity of the exponential of the linear part of the operator (obtained by setting the nonlinear part to zero). We have analyzed stability properties of ELP schemes for a class of advection–diffusion equations which includes the incompressible Navier–Stokes equations. Although the derivation remains valid for more general nonlinear partial differential equations, the exponential operator may no longer be sparse in wavelet bases. It remains an interesting problem to find sparse representations for the exponential operator of the linear part for other classes of nonlinear partial differential equations.

APPENDIX A: THE NAVIER–STOKES EQUATIONS

Let us show that the incompressible Navier–Stokes equations in three spatial dimensions can be written in the form to which considerations of this paper are applicable.

We start with the usual form of the Navier–Stokes equations for $x \in \Omega \in \mathbb{R}^3$,

$$\mathbf{u}_t = \nu \Delta \mathbf{u} - (u_1 \partial_1 + u_2 \partial_2 + u_3 \partial_3)\mathbf{u} - \nabla p, \tag{A.1}$$

$$\partial_1 u_1 + \partial_2 u_2 + \partial_3 u_3 = 0, \tag{A.2}$$

$$\mathbf{u}(x, 0) = \mathbf{u}_0, \tag{A.3}$$

(where p denotes the pressure) and the boundary condition

$$\mathbf{u}(x, t) = 0 \quad \text{on } \partial\Omega, t \in [0, T]. \tag{A.4}$$

Here we use the notation

$$\mathbf{u} = \begin{pmatrix} u_1 \\ u_2 \\ u_3 \end{pmatrix}, \quad x = \begin{pmatrix} x_1 \\ x_2 \\ x_3 \end{pmatrix},$$

and $\partial_k = \partial/\partial x_k$. Let us introduce the Riesz transforms which are defined in the Fourier domain as

$$(\widehat{R_j f})(\xi) = \frac{\xi_j}{|\xi|} \hat{f}(\xi), \quad j = 1, 2, 3, \tag{A.5}$$

where $\hat{f}$ denotes the Fourier transform of the function f. Let us consider the projection operator on the divergence-free functions,

$$\mathbf{P} = \begin{pmatrix} I & 0 & 0 \\ 0 & I & 0 \\ 0 & 0 & I \end{pmatrix} - \begin{pmatrix} R_1^2 & R_1 R_2 & R_1 R_3 \\ R_2 R_1 & R_2^2 & R_2 R_3 \\ R_3 R_1 & R_3 R_2 & R_3^2 \end{pmatrix}. \tag{A.6}$$

In order to show that $\mathbf{P}(\mathbf{u})$ satisfies (A.2), let us compose the divergence operator and (A.6), so that we need to verify

$$\begin{aligned} \partial_1 R_1^2 + \partial_2 R_2 R_1 + \partial_3 R_3 R_1 &= \partial_1 \\ \partial_1 R_1 R_2 + \partial_2 R_2^2 + \partial_3 R_3 R_2 &= \partial_2 \\ \partial_1 R_1 R_3 + \partial_2 R_2 R_3 + \partial_3 R_3^2 &= \partial_1. \end{aligned} \tag{A.7}$$

It is easy to check relations (A.7) by examining symbols of these operators in the Fourier domain; for example, the first equation in (A.7) reduces to

$$\mathrm{i}\xi_1 \frac{\xi_1^2}{|\xi|^2} + \mathrm{i}\xi_2 \frac{\xi_2 \xi_1}{|\xi|^2} + \mathrm{i}\xi_3 \frac{\xi_3 \xi_1}{|\xi|^2} = \mathrm{i}\xi_1. \tag{A.8}$$

Applying the divergence operator to (A.1), we obtain

$$-\Delta p = \sum_{k,l=1}^{3} \partial_k \partial_l u_k u_l \tag{A.9}$$

and an expression for pressure in terms of the Riesz transforms,

$$p = -\sum_{k,l=1}^{3} R_k R_l (u_k u_l). \tag{A.10}$$

Substituting (A.10) into (A.1) and taking into consideration that the Riesz transforms commute with derivatives and, moreover,

$$R_k \partial_l = R_l \partial_k, \tag{A.11}$$

we obtain

$$\mathbf{u}_t = \nu \Delta \mathbf{u} - \mathbf{P}\left(\sum_{m=1}^{3} u_m \partial_m \mathbf{u} \right), \tag{A.12}$$

instead of (A.1) and (A.2). Equations (A.12) are now in the form (2.1), where $\mathcal{L} = \nu\Delta$ and $\mathcal{N}(\mathbf{u}) = -\mathbf{P}(\sum_{m=1}^{3} u_m \partial_m \mathbf{u})$.

The transformation from (A.1) and (A.2) to (A.12) is well known and appears in a variety of forms in the literature (here we follow a derivation by Yves Meyer at the summer school at Luminy in 1997). The apparent problem with (A.12) for use in numerical computations is that the Riesz transforms are integral operators (which makes (A.12) into an integro-differential equation).

Let us point out that the presence of the Riesz transforms does not create serious difficulties if we represent operators R_j, $j = 1, 2, 3$, in a wavelet basis with a sufficient number of vanishing moments (for a given accuracy). The reason is that these operators are nearly local on wavelets (see, e.g. [5]) and, thus, have a sparse representation. This approximate locality follows directly from the vanishing moments property. Vanishing moments imply that the Fourier transform of the wavelet and its several first derivatives vanish at zero and, therefore, the discontinuity of the symbol of the Riesz transform at zero has almost no effect. The precise statements about such operators can be found in [5, 4].

Finally, in rewriting (A.12) as

$$\mathbf{u}_t = \mathcal{L}\mathbf{u} + \mathcal{N}(\mathbf{u}), \tag{A.13}$$

we incorporate the boundary conditions into the operator $\mathcal{L}$. For example, $\mathbf{u} = \mathcal{L}^{-1}\mathbf{v}$ means that u solves $\mathcal{L}\mathbf{u} = \mathbf{v}$ with the boundary conditions $\mathcal{B}u = 0$. Similarly, $u(x,t) = \mathrm{e}^{\mathcal{L}t}u_0(x)$ means that u solves $u_t = \mathcal{L}u$, $u(x,0) = u_0(x)$, and $\mathcal{B}u(x,t) = 0$.

APPENDIX B

For the convenience of the reader, we describe a technique for the computation of a marginal stability curve (or the boundary of a stability region). We start with the test problem

$$u_t = \mu u, \tag{B.1}$$

where μ is a complex parameter. Applying a time-discretization method to this equation, we obtain a homogeneous linear difference equation,

$$\sum_{k=0}^{M} (\alpha_k u_{n-k} - \mu \Delta t \beta_k u_{n-k}) = 0. \tag{B.2}$$

Setting $\lambda = \mu \Delta t$, we look for a region of (absolute) stability, which is the region in the complex λ-plane, where the solution u_n remains bounded as $n \to \infty$. The solution to (B.2) can be sought in the form $u_n = z^n$, where $z = |z|e^{i\theta}$. Evidently, the solution grows with n if $|z| > 1$ and it decays if $|z| < 1$. Hence, the boundary of the stability region is determined by the condition $|z| = 1$. Thus, to find the boundary we set

$$z = e^{\mathrm{i}\theta}. \tag{B.3}$$

By setting $\lambda = \lambda_r + \mathrm{i}\lambda_i$ and substituting (B.3) into (B.2), we arrive at a linear system

$$\begin{aligned} C\lambda_r - D\lambda_i &= A, \\ C\lambda_r + D\lambda_i &= B, \end{aligned}$$

where

$$A(\theta) = \mathrm{Re} \sum_{k=0}^{M} \alpha_k e^{i(n-k)\theta}, \quad B(\theta) = \mathrm{Im} \sum_{k=0}^{M} \alpha_k e^{i(n-k)\theta},$$

$$C(\theta) = \mathrm{Re} \sum_{k=0}^{M} \beta_k e^{i(n-k)\theta}, \quad D(\theta) = \mathrm{Im} \sum_{k=0}^{M} \beta_k e^{i(n-k)\theta}.$$

Its solution,

$$\lambda_r(\theta) = \frac{AC + BD}{C^2 + D^2}, \quad \lambda_i(\theta) = \frac{BC - AD}{C^2 + D^2},$$

is nothing else but the parametric form of the boundary of the stability region. It describes a closed curve in the plane (λ_r, λ_i), where θ sweeps the interval $0 \le \theta \le 2\pi$.

APPENDIX C

In this section we show that the family of schemes with $l = 2$ has a weak instability in the limit $q \to 0$. As an example let us analyze the third-order implicit scheme with the stability region illustrated in Fig. 4. The coefficients of this scheme are given in Table III with $M = 2$. In the limit $q \to 0$, the values of $Q_k^2 = Q_k(2q\Delta t)$ are

$$Q_1^2 = 2, \quad Q_2^2 = 2, \quad Q_3^2 = \frac{4}{3}, \quad Q_4^2 = \frac{2}{3}. \tag{C.1}$$

For the corresponding values of the coefficients we have $\gamma = 1/3$, $\beta_0 = 4/3$, $\beta_1 = 1/3$.

The linear homogeneous difference equation in this case is

$$u_{n+1} = u_{n-1} + \frac{\lambda}{3}(u_{n+1} + 4u_n + u_{n-1}), \tag{C.2}$$

where $\lambda = \mu\Delta t$. We seek the solution of (C.2) in the form $u_n = z^n$. This gives us the characteristic equation,

$$z^2 - 1 = \frac{\lambda}{3}(z^2 + 4z + 1). \tag{C.3}$$

Solving this equation with respect to λ, we obtain

$$\frac{\lambda}{3} = \frac{z^2 - 1}{z^2 + 4z + 1} = \frac{z - z^{-1}}{z + 4 + z^{-1}}. \tag{C.4}$$

Since on the boundary of the stability region $z = e^{i\theta}$, we have

$$\lambda(\theta) = -i\frac{3\sin(\theta)}{2 + \cos(\theta)}, \tag{C.5}$$

and we note that $\lambda(\theta)$ is pure imaginary for all $0 \le \theta \le 2\pi$. Thus, the boundary of the stability region in the limit $q \to 0$ is an interval of the imaginary axis. It is easy to see that the function in (C.5) has the extreme values $\pm\sqrt{3} \approx \pm 1.73$. Thus, we have $-\sqrt{3} \le i\mu\Delta t \le \sqrt{3}$ (compare with the diagram in Fig. 4 at $q = 0$).

The same consideration is applicable to the first-order explicit scheme (2.9). Using the expressions for the coefficients in Tables III and IV and the values of Q_k in (C.1), one can show that for the second-order implicit $M = 1$ and second-order explicit $M = 2$ schemes the stability region also degenerates to a line in the limit $q \to 0$. For the third-order explicit scheme the stability diagram at $q = 0$ is more complicated but still the stability region has zero thickness near the origin, $\lambda = 0$.

Thus, practical second- and third-order schemes of the class with $l = 2$ have weak instability.

APPENDIX D

Let us prove the A-stability of the implicit second-order ELP scheme with $M = 1$ and $l = 1$ used in [7],

$$u_{n+1} = e^{-q\Delta t}u_n + \mu\Delta t(\gamma u_{n+1} + \beta_0 u_0), \tag{D.1}$$

with coefficients $\gamma = \beta_0 = Q_1/2$, where

$$Q_1 = \frac{1-E}{q\Delta t}, \quad E = e^{-q\Delta t}. \tag{D.2}$$

Since we are interested in the boundary of the stability region, we seek the solution of (D.1) in the form $u_n = e^{in\theta}$. Substituting $u_n = e^{in\theta}$ into Eq. (D.1) and denoting $\lambda = \mu\Delta t$, we obtain

$$\cos\theta + i\sin\theta = E + \frac{Q_1}{2}(1 + \cos\theta + i\sin\theta)(\lambda_r + i\lambda_i). \tag{D.3}$$

By considering real and imaginary parts separately, we arrive at the system of two linear equations

$$\begin{aligned} \frac{2}{Q_1}(\cos\theta - E) &= (1+\cos\theta)\lambda_r - \sin\theta\,\lambda_i, \\ \frac{2}{Q_1}\sin\theta &= \sin\theta\,\lambda_r + (1+\cos\theta)\lambda_i, \end{aligned} \tag{D.4}$$

with the solution

$$\lambda_r = q\Delta t, \quad \lambda_i = q\Delta t\frac{1+E}{1-E}\frac{\sin\theta}{1+\cos\theta}. \tag{D.5}$$

The equation in (D.5) describes the vertical line on the complex λ-plane parallel to the imaginary axis and located at the distance $q\Delta t$ from the origin (see Fig. 6).

REFERENCES

1. B. Alpert, A class of bases in l^2 for the sparse representation of integral operators, *SIAM J. Math. Anal.* **24**(1), 246 (1993).
2. B. Alpert, G. Beylkin, D. Gines, and L. Vozovoi, Toward adaptive solution of partial differential equations in multiwavelet bases, in progress.
3. U. M. Ascher, S. J. Ruuth, and B. T. R. Wetton, Implicit–explicit methods for the time dependent partial differential equations, *SIAM J. Numer. Anal.* **32**(3), 797 (1995).
4. G. Beylkin, On the representation of operators in bases of compactly supported wavelets, *SIAM J. Numer. Anal.* **29**(6), 1716 (1992).
5. G. Beylkin, R. R. Coifman, and V. Rokhlin, Fast wavelet transforms and numerical algorithms I, *Comm. Pure and Appl. Math.* **44**, 141 (1991). [Yale University Technical Report YALEU/DCS/RR-696, August 1989]
6. G. Beylkin, R. R. Coifman, and V. Rokhlin, Wavelets in numerical analysis, in *Wavelets and Their Applications* (Jones & Bartlett, Boston, 1992), p. 181.
7. G. Beylkin and J. M. Keiser, On the adaptive numerical solution of nonlinear partial differential equations in wavelet bases, *J. Comput. Phys.* **132**, 233 (1997). [PAM Report 262, 1995]
8. G. Dahlquist and A. Björck, *Numerical Methods* (Prentice-Hall, Englewood Cliffs, NJ, 1974).
9. U. Frish, Z. S. She, and O. Thual, Viscoelastic behaviour of cellular solutions to the kuramoto-sivashinsky model, *J. Fluid Mech.* **168**, 221 (1986).
10. C. W. Gear, *Numerical Initial Value Problems in Ordinary Differential Equations* (Prentice-Hall, Englewood Cliffs, NJ, 1973).

11. M. Hochbruck and C. Lubich, On Krylov subspace approximations to the matrix exponential operator, *SIAM J. Numer. Anal.* **34**(5), 1911 (1997).
12. A. Iserles, *A First Course in the Numerical Analysis of Differential Equations* (Cambridge Univ. Press, Cambridge, 1996).
13. M. K. Jain and V. K. Srivastava, *High Order Stiffly Stable Methods for Ordinary Differential Equations*, Technical Report 394, University of Illinois, Urbana, II, 1970.
14. G. E. Karniadakis, M. Israeli, and S. A. Orszag, High order splitting methods for the incompressible Navier–Stokes equations, *J. Comput. Phys.* **97**, 414 (1991).